Cellular Structures in the Flow Over the Flap of a Two-Element Wing

Steven A. Yon and Joseph Katz

Department of Aerospace Engineering and Engineering Mechanics

SDSU, San Diego, CA

ABSTRACT

Flow visualization information and time dependent pressure coefficients were recorded for the flow over a two-element wing. The investigation focused on the stall onset; particularly at a condition where the flow is attached on the main element but separated on the flap. At this condition, spanwise separation cells were visible in the flow over the flap, and time dependent pressure data was measured along the centerline of the separation cell. The flow visualizations indicated that the spanwise occurrence of the separation cells depends on the flap (and not wing) aspect ratio.

INTRODUCTION

Surface flow visualization experiments at high angles of attack on rectangular wings showed the existence of organized spanwise cellular patterns, which appear during early post stall condition (Ref. 1 - 3). Those patterns seem to form immediately at the onset of stall and tend to diminish as angle of attack increases. The number of cells depends on wing aspect ratio, with a single cell aspect ratio of about 1.5 to 2.5 (Ref. 2, 4). Measurements of the wing surface pressure fluctuations while the above cellular patterns were visible showed that one of the dominant frequencies is much lower (Ref. 4) than the expected Strouhal frequency (of $St = \omega c/V_\infty = 0.15$). Such information may affects airplane wing design since the natural vibration modes should not coincide with the dominant aerodynamic frequencies.

Those considerations are even more pronounced with extended flap systems where the additional flexibility leads to larger vibration levels. Therefore, the main objective of this study is to demonstrate the existence of cellular patterns on the stalled flap, during the initial stages of stall, when the flow on the main wing element is still attached. Also, the spanwise spacing of the separation cells is addressed to determine whether it depends on the whole wing's or on the flap's aspect ratio only. Time dependent surface pressure variations were measured to provide experimental data for future numerical validations of turbulent separated flows, and to determine if the measured reduced frequency can be scaled based on the whole wing or on the flap-chord only.

EXPERIMENTAL SETUP

The photograph of the wing as mounted in the wind tunnel is shown in Fig. 1, and its side view in Fig. 2. The main wing plane was kept at zero angle of attack and the flap angle varied between 30, 35, and 40 deg. Surface tufts were used for flow visualization, and in the photograph in Fig. 1, two separation-cells may be observed. The two element wing was held by large Plexiglas end-plates to simulate (as closely as possible) 'two-dimensional' flow conditions. The wing, flap, and end-plate assembly were mounted inside a 1.14 m wide, 0.81 m tall and 1.66 m long test section. Additional details on model geometry are presented in Fig. 2. Airspeed was set at V_∞ = 53.6 m/sec, resulting in a Reynolds number of 1.28 x 10^6 based on the wing's combined chord (including the flap). The shape of the main airfoil element is based on the NACA four-digit family, with maximum thickness t/c=0.18, max. camber/c=0.12, and location of max. camber at x/c=0.425 (see Ref. 5. p.114, on using these values to define the airfoil shape). The flap shape is based on a symmetric NACA 0015 airfoil section. Time dependent pressure measurements were obtained by small (Endevco, 5 mm diameter, and 1 mm^2 active area) piezo-resistive transducers embedded along the flap's chord. The absolute pressure range of the transducers is from 0 to about one atm with a resolution of 0.17 x 10^{-4} atm, and maximum frequency response of about 0.15 MHz. The

flap section containing the transducers was free to move laterally along the flap span. However, for the present data it was kept at the visual centerline of the left separation cell.

RESULTS

As stated earlier, the focus of this investigation was on the condition where the flow is attached on the main wing element but separated on the flap. Therefore, subsequent to a brief flow visualization experiment to determine the desirable test conditions, the main element orientation was set at zero angle of attack and only the flap angle δ_f varied. Flap stall was observed at $\delta_f = 40^0$, but at $\delta_f = 30^0$ the flow on the flap was still attached. At this stalled flap condition ($\delta_f = 40^0$), two stable separation cells were visible on the flap, as shown in Fig. 1. Note that all tufts had the same length; therefore near the centerline the flow is attached and further out the flow is reversed (the fluttering of the tufts was easily visible during the test but was not entirely captured by this still photograph). The aspect ratio of a single separation cell, based on the flap dimensions, is about 2, which is close to the values observed on single element wings (Ref. 1, 2). Since the wind-tunnel model layout resembled a two-dimensional experiment, one of the widely used two-dimensional airfoil-design codes (MSES - Ref. 6) was used for comparison purposes. Results of these computations, in terms of the streamlines near the airfoil and with the measured chordwise pressure distribution, for the two flap deflections, is shown in Fig. 3 and Fig. 4. The circular symbols stand for the time average pressure coefficient measured on the flap. Clearly, at the lower flap deflection the flow is attached (as indicated by the stationary tufts during the flow visualization) and the computed and measured pressures on the flap are satisfactorily close. The computations also show a laminar bubble near the midchord of the main element; and for such attached flow conditions the computed results should be close to the actual flow conditions.

Data similar to Fig. 3, but for a larger flap deflection of $\delta_f = 40^0$ is shown in Fig. 4, and the computed streamlines show an early flow separation on the flap. As mentioned earlier, the flow visualization experiments showed two cellular separation cells on the upper surface (Fig. 1) and the calculated two-dimensional separation point may be wieved as an avarage representation of the three-dimensional phenomenon. The experimental pressure coefficient data in this figure was measured along the center of the left separation cell and does not compare well with the computed results. The shape of the measured pressure distribution on the flap is quite flat (typical stall) whereas the computations still show a large leading edge suction. Similar pressure measurements in-between the separation cells, but with a single element wing (Ref. 4), showed typical attached flow pressure distributions with large leading edge suction. However the magnitude of the measured data was much smaller than estimated by two-dimensional computations, suggesting an effectively lower angle of attack condition there due to the downwash created by the adjacent stall cells. Thus, although the test attempts to enforce two-dimensional condition, the separated flow is naturally time dependent and three dimensional (with significant spanwise variations) and any attempt to compare with two-dimensional computations may lead to similar discrepancies.

The time dependent pressure fluctuations, as measured by the five chordwise transducers on the flap are shown for a flap deflection of $\delta_f = 30^0$ in Fig. 5 (transducer #1 is closest to the leading edge and #5 is near the trailing edge). The data presented includes the time dependent component only (with an average value of Cp=0) which is obtained by subtracting the time average value. Similar measurements on the stalled flap at $\delta_f = 40^0$ show a large increase in the amplitude of the pressure fluctuations (Fig. 6). The general characteristics of the separated-flow pressure fluctuations has a more complicated structure than the more periodic signal measured with the attached flow (Fig. 5). This observation is true for all five chordwise transducers and the amplitudes seem to grow towards the flap trailing edge. This growth of the disturbance towards the trailing edge is present in Fig. 5 as well, but at a much

smaller magnitude. Of course, having a time dependent description of the actual small-scale vortices within the separated flow, their structures and transport properties, might have determined the source of the above fluctuations. However, in the absence of such detailed information, the use of some statistical tools may prove useful. Therefore, the power spectra density (PSD) estimates for the time history of the pressure coefficients in Fig. 5 and Fig. 6 are shown in Fig. 7. The most dominant frequency is about 117 Hz and the amplitudes in general increase towards the trailing edge (as discussed earlier). A closer look at the test facility reveals that the wind tunnel fan has four blades and it rotates at 1750 RPM; which may create a prevalent excitation of about 117 Hz. Indeed, Fig. 7 shows that the power is centered near this 'driving' frequency and is considerably amplified in the case of the separated flow. The largest fluctuation in the pressure history in Fig. 6 are clearly responsible for the peak power in Fig. 7 and are due to the unsteady separated flow since the baseline (in Fig. 5) contains nothing similar. Crosscorelation between the signals of the individual transducers suggests streamwise convection of the strong periodic component shown in Fig 6, at about half the free-stream velocity. Estimating the Strouhal number, based on the frontal height of the separated area of the flap yield St ~ 0.13, which is quite close to results obtained with single element wings. Also, in these tests a 50 Hz high-pass filtering was applied to minimize tunnel vibration effects that occur near 30 Hz. In spite of this filtering, sizable power under the 50 Hz range is visible for the $\delta_f = 40^0$ case (especially for transducer 1) which effect is not present at the attached flow on flap case. This indicates that the lower frequency fluctuations within the separated flow as reported in Ref. 4 and Ref. 7 are present here as well (but was mostly filtered out by the 50 Hz high-pass filter). Finally, when comparing the power generated in the separated flow case with the one in the attached flow case in the PSD diagram of Fig. 7, the effect of flow separation becomes evident. It seems that the Strouhal type periodic vortex flow that develops in the separated flow, at the $\delta_f = 40^0$ case, causes the sharp increase in the pressure fluctuations. Also, the expected natural frequency of the vortex flow is quite close to the fan-blade passage frequency, and

similarly to the mechanical vibration case, the flow frequency 'adopts' and magnifies the prevailing (forcing) frequency within the free-stream.

CONCLUDING REMARKS

The presence of the spanwise separation cells on the stalled flap of a two element wing with attached flow on the main element was demonstrated. The aspect ratio (≈ stall cell span/flap chord) is on the order of 2, which is close to the values reported for single element airfoils. Also, when scaling the dominant pressure fluctuation frequencies observed on the flap, based on the flap chord, the resulting Strouhal number is close to values measured on single element, stalled wings. When observing the power of the pressure fluctuations in the frequency domain; the frequency of the largest pressure fluctuations, caused by the separated flow, drifted close to the wind tunnel driving frequency (much like in the case of simple mechanical vibrations). This experiment also demonstrates the difficulties in obtaining time dependent information on the actual three dimensional structures within the flow above a wing when using surface information only. Thus, real flows are neither two-dimensional or quasi steady but rather three-dimensional and time dependent.

ACKNOWLEDGMENTS

This work was funded through NASA Ames Research Center Joint Research Consortium Agreement No. NCA2-786, with James Ross as project monitor.

REFERENCES

1.Gregory, N., V. G. Quincy, C. L. O'Reilly, and D. J. Hall 1970 "Progress Report on Observations of Three Dimensional Flow Patterns Obtained During Stall Development on Aerofoils, and on the Problem of Measuring Two-Dimensional Characteristics," Aeronautical Research Council, Fluid Motion Sub-Committee, 31 702, NPL Aero Report 1309.

2.Winkelmann, A. E., and J. B. Barlow 1980 "Flowfield Model for a Rectangular Planform Wing Beyond Stall," *AIAA Journal,* Vol. 18, No. 8, pp. 1006-1008.

3.Weihs, D., and J. Katz 1983 "Cellular Patterns in Poststall Flow over Unswept Wings," *AIAA Journal,* Vol. 21, No. 12, pp. 1757-1758.

4.Yon, S., and Katz, J., "Study of the Time Dependent Flow on a Stalled Wing," AIAA paper 97-xxxx, presented at the 28th AIAA Fluid Dynamics Conf., Snowmass, CO, June/July 1997.

5.Abbott, I. H. and von Doenhoff, A. E. "Theory of Wing Sections", Dover, New York, 1959.

6.Drela, M., "Design and Optimization Method for Multielement Airfoil Flow, " AIAA . Paper 93-0969, Feb., 1993.

7.Zaman, K. M. B. Q., D. J. McKinzie, and C. L. Rumsey 1989 "A Natural Low-Frequency Oscillation of the Flow Over an Airfoil Near Stalling Conditions," *Journal of Fluid Mechanics,* Vol. 202, pp. 403-442.

8. Yon, S. A., 1995, "Coherent Structures in the Wake of a Stalled Rectangular Wing," Ph.D. Thesis, University of California, San Diego, and San Diego State University.

Figure captions

Fig. 1 The two element wing, as mounted in the wind-tunnel test section. Flap angle is δ_f = 40^0 and the tufts show two separation cells on the flap.

Fig. 2 Geometry of the two-element wing as mounted in the test section (dimensions in m).

Fig. 3 Computed two-dimensional pressure distribution (using the method of Ref. 6) for the two element wing at $\delta_f = 30^0$. The circular symbols show the five measured steady state flap-pressures along the separation cell centerline.

Fig. 4 Computed two-dimensional pressure distribution (using the method of Ref. 6) for the two element wing at $\delta_f = 40^0$. The circular symbols show the five measured steady state flap-pressures along the separation cell centerline.

Fig. 5 Time history of pressure coefficients as measured by the 5 transducers along the flap chord, for $\delta_f = 30^0$ (attached flow). Note; $(x/c)_{flap}$ is normalized by flap chord, which is about 65% of the main element chord.

Fig. 6 Time history of pressure coefficients as measured by the 5 transducers along the flap chord, for $\delta_f = 40^0$ (separated flow).

Fig. 7 Power spectral density estimates for the pressure coefficient time histories at flap settings of $\delta_f = 30^0$ (broken lines) and $\delta_f = 40^0$ (solid lines). Note; transducer No. 1 closer to the leading edge and No. 5 is near the trailing edge.

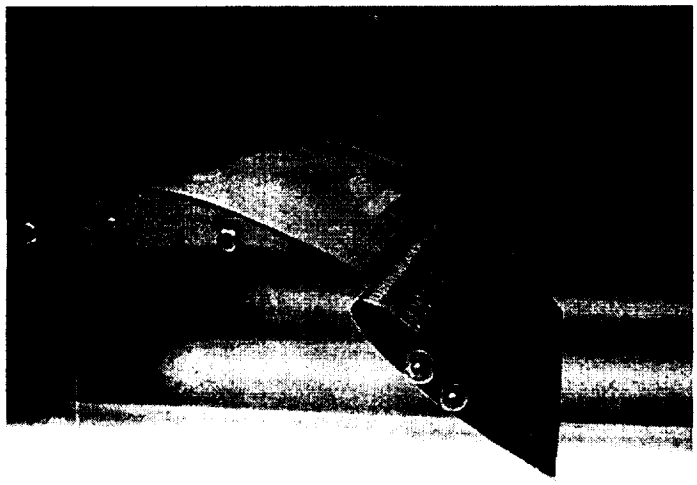

Fig 1

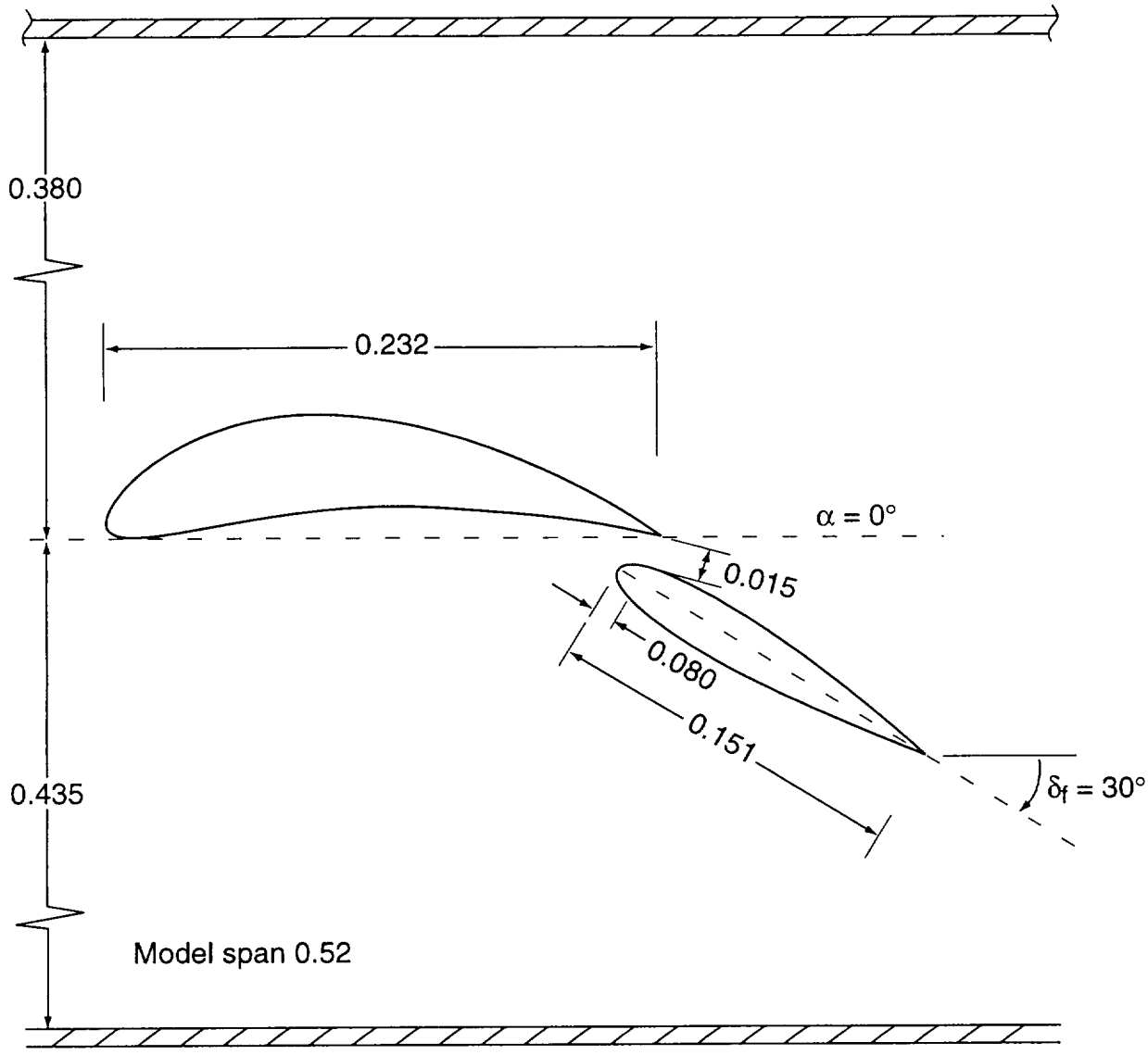

Fig 2

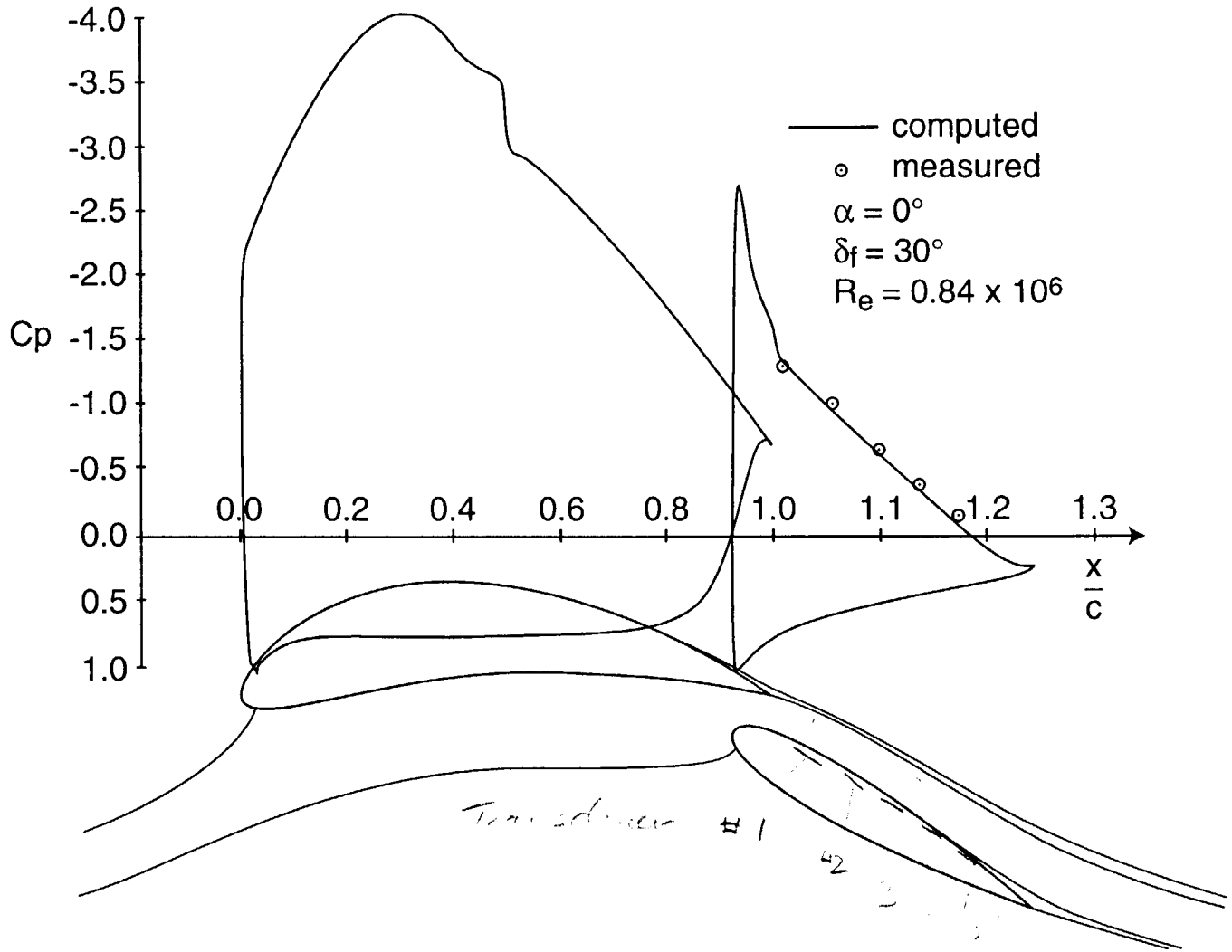
-4.0
-3.5
-3.0
-2.5
-2.0
-1.5
-1.0
-0.5
0.0
0.5
1.0
Cp
0.0
0.2
0.4
0.6
0.8
1.0
1.1
1.2
1.3
x/c
computed
measured
α = 0°
δf = 30°
Re = 0.84 x 10^6

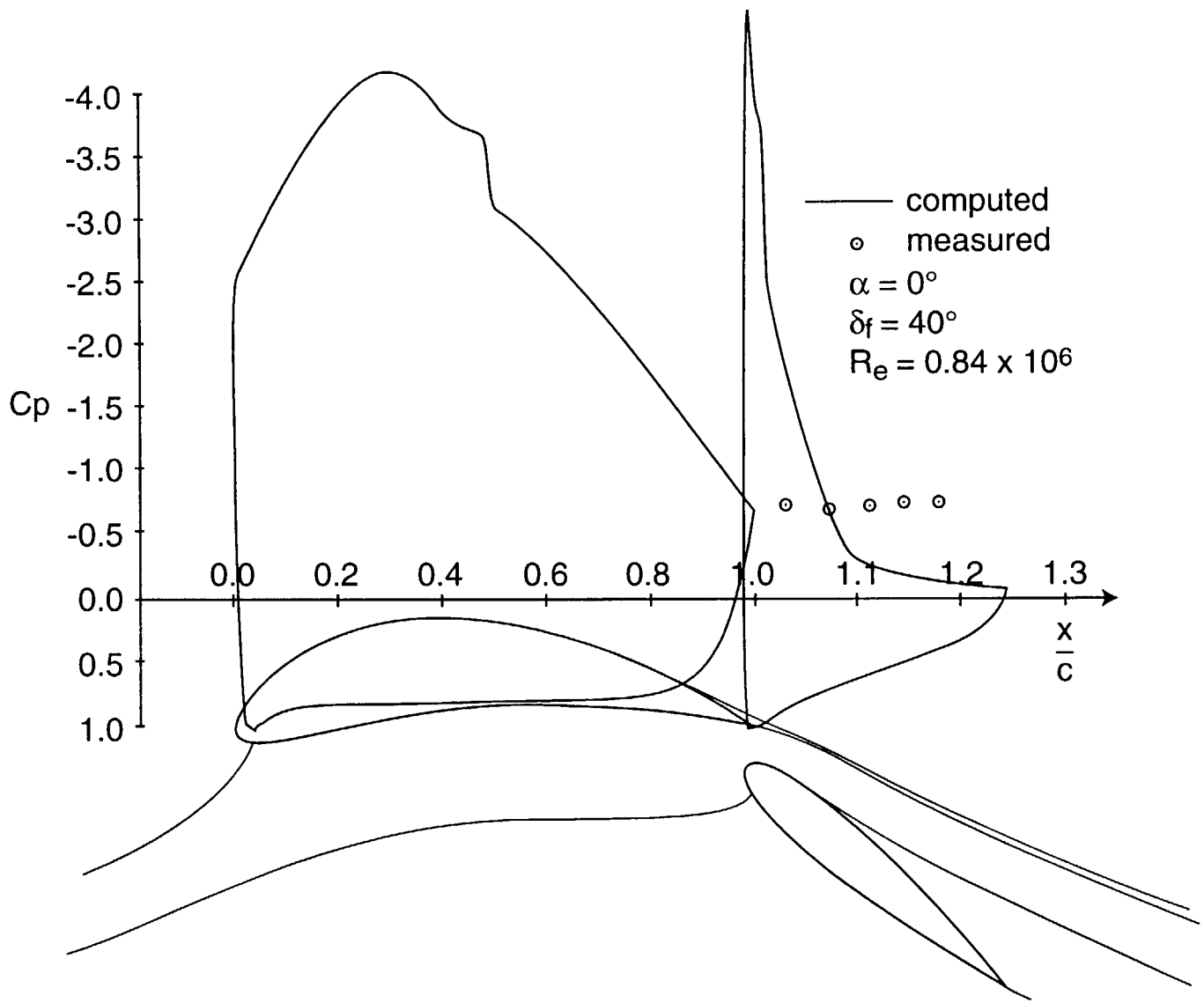
-4.0
-3.5
-3.0
-2.5
-2.0
Cp -1.5
-1.0
-0.5
0.0
0.5
1.0
0.0
0.2
0.4
0.6
0.8
1.0
1.1
1.2
1.3
x/c
computed
measured
α = 0°
δf = 40°
Re = 0.84 x 10^6

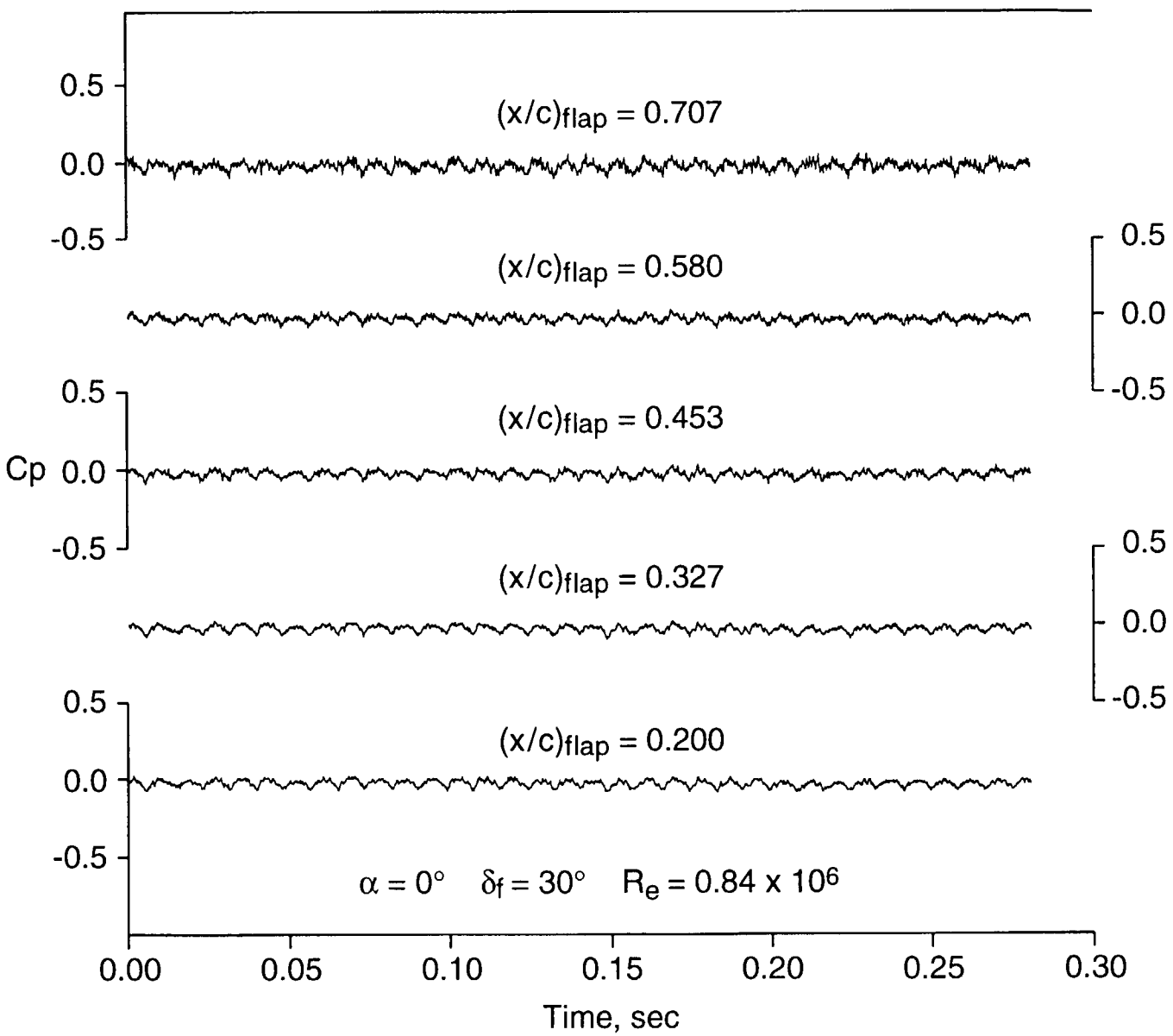
0.5
0.0
-0.5
(x/c)flap = 0.707
(x/c)flap = 0.580
(x/c)flap = 0.453
(x/c)flap = 0.327
(x/c)flap = 0.200
Cp
α = 0°
δf = 30°
Re = 0.84 x 10^6
0.00
0.05
0.10
0.15
0.20
0.25
0.30
Time, sec

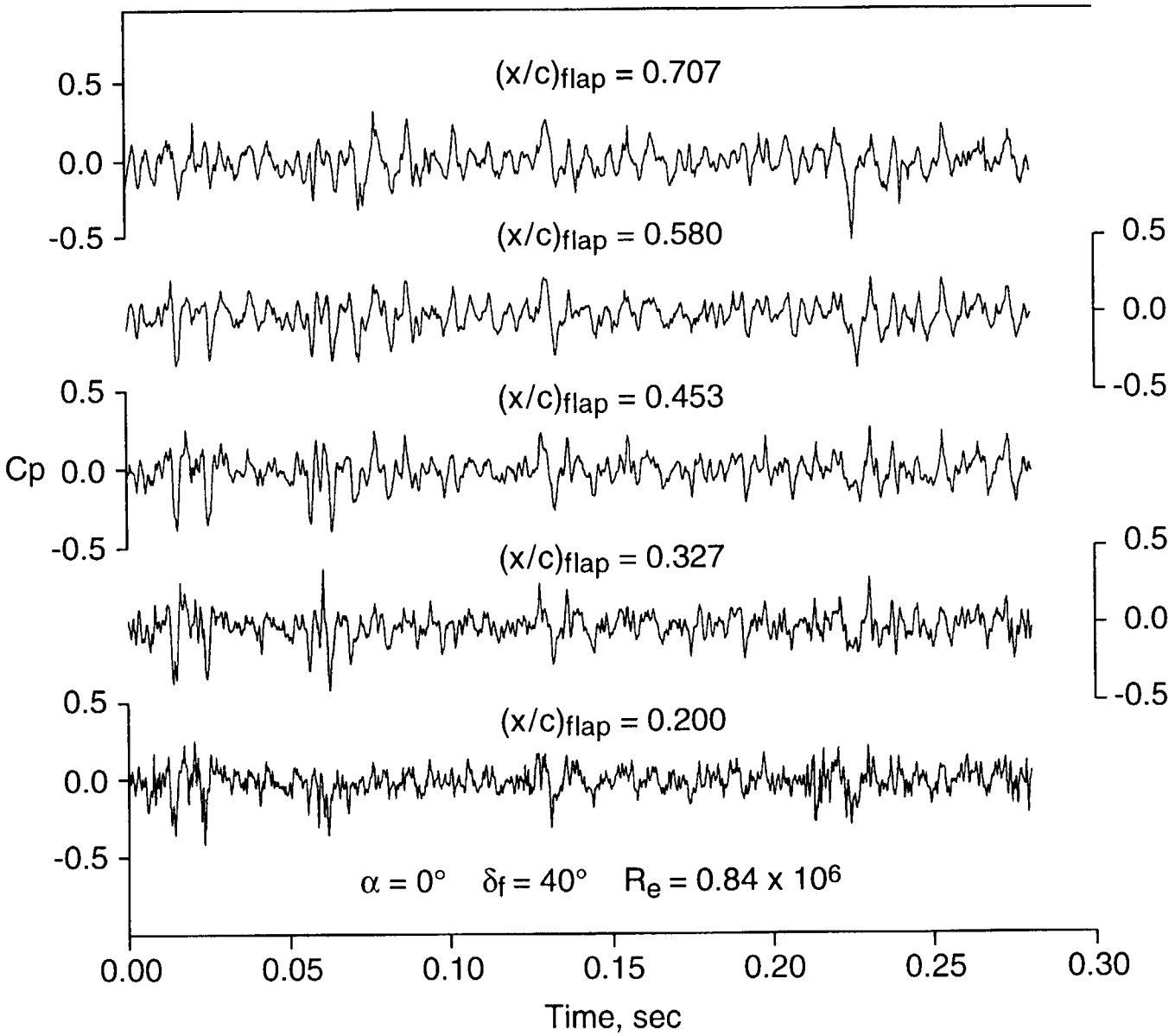
(x/c)flap = 0.707
(x/c)flap = 0.580
(x/c)flap = 0.453
(x/c)flap = 0.327
(x/c)flap = 0.200
0.5
0.0
-0.5
Cp
α = 0°
δf = 40°
Re = 0.84 x 10^6
0.00
0.05
0.10
0.15
0.20
0.25
0.30
Time, sec

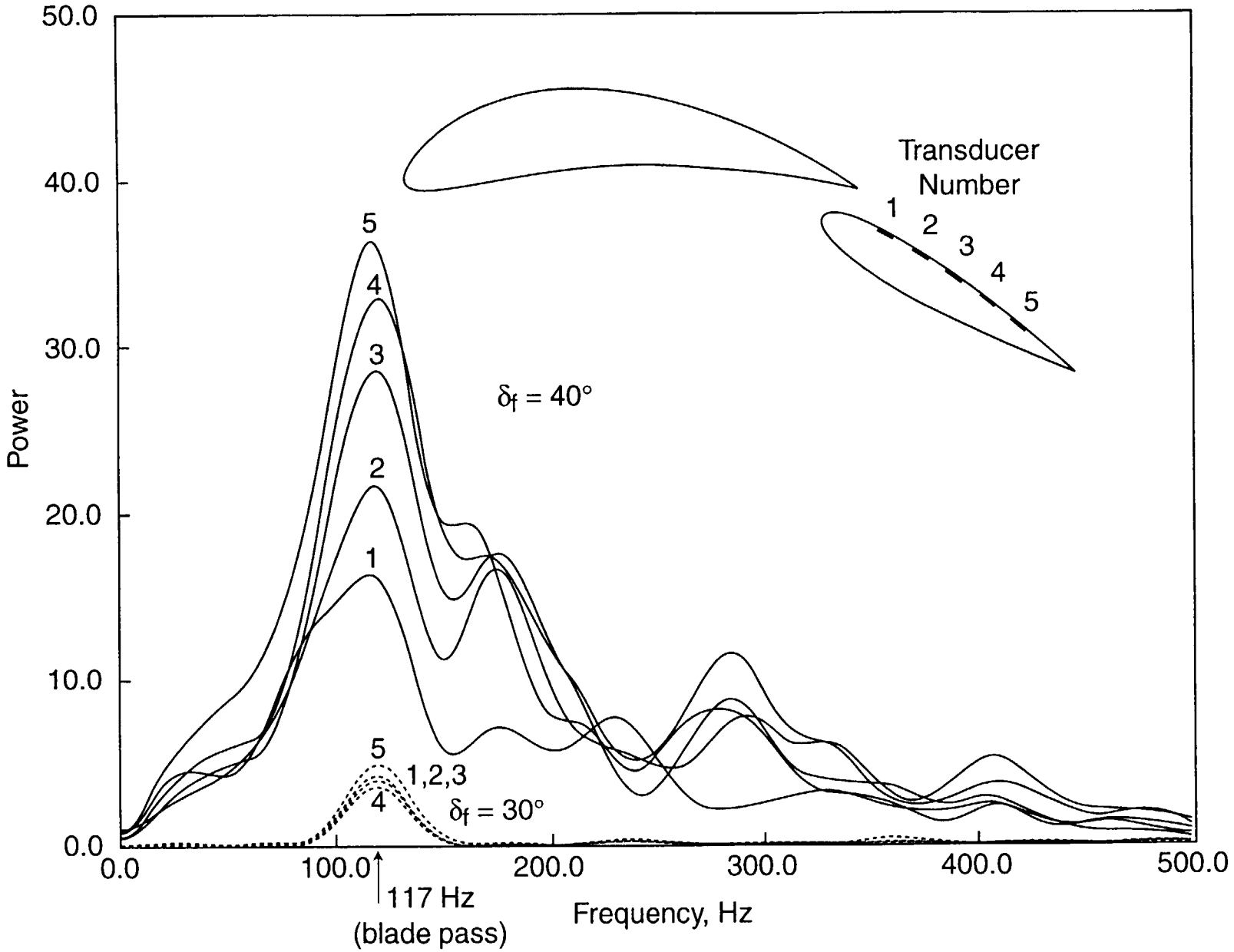
50.0
40.0
30.0
20.0
10.0
0.0
Power
0.0
100.0
200.0
300.0
400.0
500.0
Frequency, Hz
117 Hz
(blade pass)
Transducer
Number
1
2
3
4
5
δ_f = 40°
δ_f = 30°
1,2,3